Article ID: 1007-4627(2024) 00-0001-07

Effect of defects on magnetic properties of O^+-implanted AlN films by positron annihilation spectroscopy

Run YE[1], Bangjiao YE[2]

(*1. School of Physics and Electronic Engineering, Yancheng Teachers University, Yancheng 224007, China;*
2. State Key Laboratory of Particle Detection and Electronics, University of Science and Technology of China, Hefei 230026, China)

Abstract: Room-temperature ferromagnetism is observed in the O^+-implanted AlN films with O^+ doses of 5×10^{16} cm^{-2} (AlN:$O_{5\times10^{16}}$) and 2×10^{17} cm^{-2} (AlN:$O_{2\times10^{17}}$). The observed magnetic anisotropy indicate that the ferromagnetism is attributed to the intrinsic properties of O^+-implanted AlN films. The out-of-plane saturation magnetization (M_S) of the AlN:$O_{5\times10^{16}}$ is about 0.68 emu/g, much higher than that of AlN:$O_{2\times10^{17}}$, 0.09 emu/g, which is due to the excessively high O^+ dose made more O^+ ions occupy adjacent Al^{3+} positions in forms of antiferromagnetic coupling. Doppler broadening of positron annihilation radiation measurements demonstrate the existence of Al vacancies in the O^+-implanted AlN films. The first-principles calculations suggest that the ferromagnetism originates mainly from the Al vacancies. Meanwhile,the formation of divacancies or vacancy clusters by high concentrations of Al vacancies will lead to the transformation of V_{Al}–V_{Al} coupling from ferromagnetim to antiferromagnetimm, ultimately weakening the ferromagnetism of the sample.

Key words: positron annihilation spectroscopy; ion implantation; semiconductors; ferromagnetism
CLC number: O77+1 **Document code:** A **DOI:** 10.11804/NuclPhysRev.00.01.01

1 Introduction

AlN, a wide-bandgap III-V semiconductor, has attracted much attention in the last decade for its high thermal conductivity, high electron mobility, and good chemical stability[1-2]. The induced magnetism in AlN make it posiible to manipulate the charge and spin degrees of freedom of an electron in AlN simultaneously. Thus, AlN is a promising cadidate in spintronics[3] and become a diluted magnetic semiconductor (DMS) when doped with transition metals inducing ferromagnetism[4-6].

Recently, ferromagnietism was observed in AlN with non-magnetism dopants such as Cu[7], Mg[8], and C[9]. As the most common element, Oxygen can easily become an impurity in the sample, thus affecting the properties of sample. However, the magentic O-doped AlN has rarely been investigated[10]. Gennerally speaking, AlN films doped with non-magnetism dopants or transition metals ofen contains a large number of defects, and the defects are not evenly distributed, especially doping by ion implantation. It's of great importance for the origin of feromagnetism in AlN DMS films to probe the defect structure and identify the defect types.

Positron annihilation spectroscopy has turned out to be a unique method to investigate nanometer-scaled defects in materials[11-12]. By controlling the energy of incident positron, depth profile of samples can be obtained by detect the annihiltion gamma rays. A high-purity Ge detector was applied to detecte γ rays produced by the positron annihilation to reconstruct th Doppler broadening of annihilation radiation (DBAR) spectroscopy. The obtained DBAR spectrum was characterized by S and W parameters. The S parameter is defined as the ratio of central area of annihilation peak (511 ± 0.81 keV) to the total peak area, re-

Received date: 01 Apr. 2024; **Revised date:** 01 Apr. 2024
Foundation item: National Key R&D Program of China (2019YFA0210000); Natural Science Foundation of China (12305333); State Key Laboratory of Particle Detection and Electronics (SKLPDE-KF-202114); Fundamental Research Program of Yancheng City (YCBK2023061); Innovation and Entrepreneurship Doctors of Jiangsu Province (JSSCBS20211148); Natural Science Foundation of Jiangsu Province (BK20220699)
Biography: Run YE (1991–), Huanggang, Hubei Province, Lecturer, Working on positron annihilation spectroscopy; E-mail: yer@yctu.edu.cn
Corresponding author: E-mail: bjye@ustc.edu.cn

flecting the information of positron annihilation with low-momentum electrons (valence electron or conduction electron). The W parameter is the ratio of wing area (505.92-509.16 keV, 512.84-516.08 keV) to the total peak area, which reflects the information of positron annihilation with high-momentum electrons (core electrons). When positrons are captured by vacancy-type defects in samples, the S parameter increases and W parameter decreases due to the higher faction of valance electrons around defects than those in defect-free regions. Taking anvatages of DBAR measurements, the defect distribution of AlN films can obtained. In this work, we prepared O^+-doped AlN films by ion implantation and investigated the structural and magnetic properties of O^+-implanted AlN films.

2 Experiment

1-μm thick unintentionally doped AlN films (marked as as-grown AlN) prepared on c-plane (0001) sapphire substrates (~500 μm thick) by hydride vapor phase epitaxy were purchased from Hefei Kejing Materials Technology Co., Ltd. The AlN:$O_{5\times10^{16}}$ and AlN:$O_{2\times10^{17}}$ (the subscript denotes the dose of implanted O^+ ions in cm^{-2}) were obtained by implanting O^+ ions with energy of 80 keV into two as-grown AlN films. The ion implantation experiments were performed using an ion implanter at room temperature. The base pressure of implantation chamber was about 2×10^{-4} Pa at room temperature.

The crystal structure analysis was conducted by using an X-ray diffractometer (PANalytical X'Pert PRO MPD) in Bragg-Brentano geometry (240 mm radius) with Cu-Kα radiation (λ = 1.5406 Å). The Raman spectra were measured at room temperature by using a LabRamHR Evolution Raman system with an Ar ion laser (wavelength centered at 514.5 nm) in backscattering geometry as a excitation source. The Doppler broadening of annihilation radiation (DBAR) measurements were performed using a slow positron beam with a variable energy from 0.25 to 25 keV at the University of Science and Technology of China. The magnetic properties of AlN films were investigated using a Superconducting Quantum Interference Device (MPMS3, Quantum Design) with an accuracy of 10^{-8} emu. The magnetic hysteresis loop measurements were carried out at room temperature with magnetic field parallel and perpendicular to the sample's plane, respectively.

3 Results and discussion

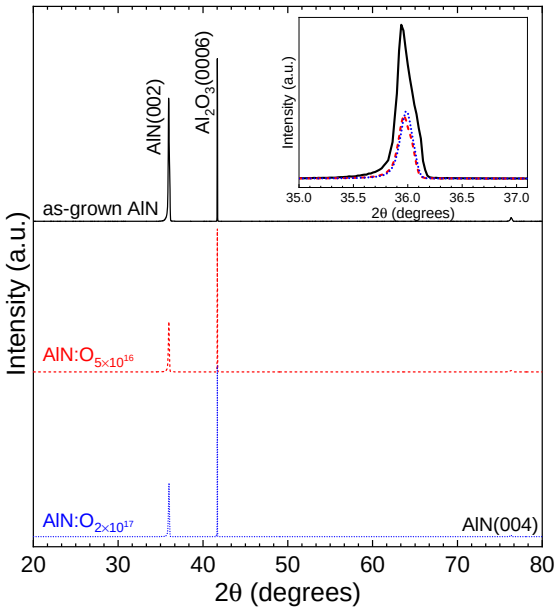

Fig. 1 (Color online) XRD patterns of AlN, AlN:$O_{5\times10^{16}}$, and AlN:$O_{2\times10^{17}}$. The inset shows the magnification of AlN (002) peaks.

Table 1 XRD results of the AlN samples.

Sample	Peak positron (°) (002)	c parameter (Å)
as-grown AlN	35.95	4.992
AlN:$O_{5\times10^{16}}$	35.96	4.991
AlN:$O_{2\times10^{17}}$	35.98	4.988

The crystal structures of the AlN samples were investigated by XRD. The XRD spectra were normalized with respect to the intensity of the (0006) peak of the sapphire substrate for as-grown AlN sample. As shown in Fig. 1, the typical (002) peaks of AlN are observed, which can be indexed to h-AlN. No peaks related to metallic Al are found in the AlN patterns. As shown in the inset of Fig. 1, the intensity of (002) peak was reduced after ion implantation, indicating that the ion implantation process introduced lots of lattice defects in AlN:$O_{5\times10^{16}}$ and AlN:$O_{2\times10^{17}}$. The XRD results of the AlN samples are shown in Table 1. The AlN (002) peak shifts towards larger 2θ after implation, suggesting a lattice constraction along the c-axis for AlN micro-crystals in AlN:$O_{5\times10^{16}}$ and AlN:$O_{2\times10^{17}}$, which is likely attributed to the substitution of N^+ or Al^{3+} by the O^+ ions due to the smaller covalent radius of O[13].

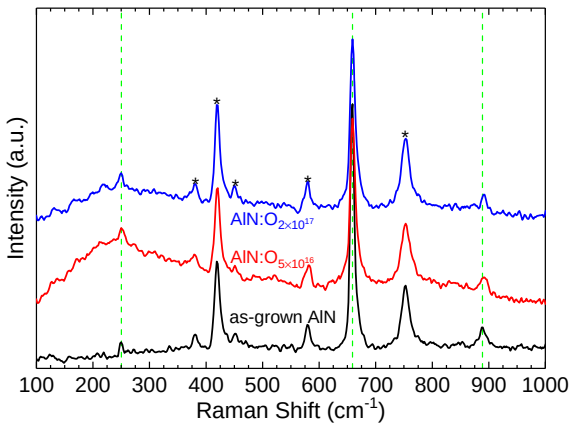

Fig. 2 (Color online) Raman spectra for as-grown AlN, AlN:$O_{5\times10^{16}}$, and AlN:$O_{2\times10^{17}}$. The asterisks represent vibrational modes related to the sapphire substrate. The green dotted lines represent the first-order phonon modes of AlN E_2 (low), E_2 (high), and A_1 (LO), respectively.

The Raman spectra of as-grown AlN, AlN:$O_{5\times10^{16}}$, and AlN:$O_{2\times10^{17}}$ are shown in Fig. 2. For as-grown AlN, first-order phonon modes located at 250 cm^{-1} [E_2 (low)], 659 cm^{-1} [E_2 (high)], and 889 cm^{-1} [A_1 (LO)] were observed, which are in good agreement with the values measured for the AlN films[14-15]. Other five peaks (marked as asterisks) are attributed to vibrational modes from the sapphire substrate.

For AlN:$O_{5\times10^{16}}$ and AlN:$O_{2\times10^{17}}$, the E_2 (high) peaks located at 659 cm^{-1} were also seen clearly in Fig. 2. The FWHM of E_2 (high) peak for as-grown AlN, AlN:$O_{5\times10^{16}}$, and AlN:$O_{2\times10^{17}}$ are about 7.4, 11.1, and 12.1 cm^{-1}, respectively. The E_2 (high) peak broadens after O^+ implantation, suggesting that there are high density defects in AlN:$O_{5\times10^{16}}$ and AlN:$O_{2\times10^{17}}$. With increasing O^+ concentration, the intensity of E_2(high) peak decreases, and the peak becomes asymmetric, indicating the lattice distortion of AlN wurtzite structure. What's more, the E_2 (low) and A_1 (LO) components in AlN:$O_{5\times10^{16}}$ and AlN:$O_{2\times10^{17}}$ disappear, broad bands emerge instead. In general, the broadening in Raman band and absence of local vibrational modes are associated with the lattice disorder, defects, and substitutional impurities, which can lead to photon confinement and loss of periodicity[16-17]. The vacancies and substitution of O^+ ions for N^+ or Al^{3+} ions are responsible for the changes in peak shape mentioned above.

Fig. 3 (a) shows the S parameters versus positron energy (S-E curves) measured for AlN films. For as-grown AlN, the positron energy of 0-2 keV is corresponding to the surface layer. The large S parameters is due to the positron

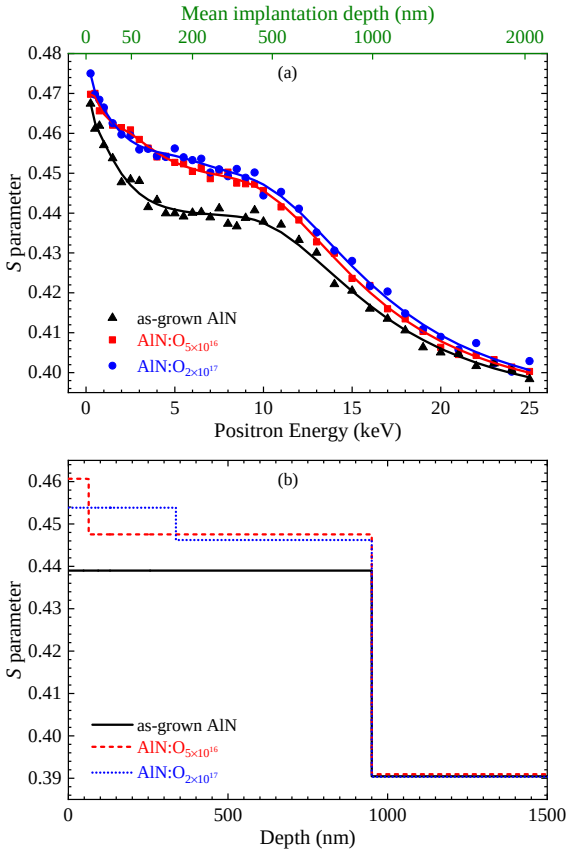

Fig. 3 (Color online) (a) The parameter S as a function of positron energy (E) for the samples. Solid lines are fitted to the experimental data by VEPFIT software. (b) S depth distributions obtained from analysis of S–E curves for the samples.

annihilations and formation of positronium atoms at the surface[18]. In the suface layer, S parameters decrease with increasing positron energy. The S values saturate at positron energy of 2-10 keV, indicating that positrons annihilate in the AlN layer. The obtained bulk S parameter (S_b) for as-grown AlN is about 0.439. Then the S parameters decrease in the energy region $E > 10$ keV due to the annihilation of positrons in the sapphire substrate. Compared to as-grown AlN, the O^+ implanted AlN films show much higher S parameters in the whole energy range, which is attributed to the annihilate of positrons in positron trapping centers in AlN are Al-related vacancies (negative charges).The defect types in AlN:$O_{5\times10^{16}}$ and AlN:$O_{2\times10^{17}}$ can be determined by S parameter. The S values for the defect layer (S_d) in AlN:$O_{5\times10^{16}}$ (AlN:$O_{2\times10^{17}}$) is 0.461 (0.454), then the value of S_d/S_b is approximately 1.050 (1.034), which indicates the implantation induced defects in AlN:$O_{5\times10^{16}}$ and AlN:$O_{2\times10^{17}}$ are probably mono-vacancies (V_{Al}) or divacancies according to previous

reports.[19-20].

To further investgate the positron annihilation characteristcs in the AlN films, the $S-E$ curves were fitted using VEPFIT software[21] to resolve the defect depth profiles and depth structures of implanted AlN layers. The S parameter measured at different positron energy E can be expressed by the following formula:

$$S(E) = S_S F_S(E) + \sum_{i=1}^{n} S_i F_i(E) \quad (1)$$

where S_S and S_i are the S parameters to the positrons annihilated at the surface and in the ith layer, respectively; while, F_S and F_i denote the fraction of positrons annihilated at the surface and in the ith layer the with the relation of $F_S(E) + \sum_{i=1}^{n} F_i(E) = 1$, respectively. As shown in Fig. 3 (a), the solid lines are in accord with the experiment data. According to the previous work[22], the region exposed to annihilated positrons was divided into two blocks for as-grown AlN, and three blocks for AlN:$O_{5\times10^{16}}$ (AlN:$O_{2\times10^{17}}$), respectively. The defect depth profiles for the AlN films are shown in Fig. 3 (b). In the first block of ~60 nm, AlN:$O_{5\times10^{16}}$ and AlN:$O_{2\times10^{17}}$ exhibit high S values due to the ion implantation and high O^+ concentration. However, the S value of AlN:$O_{5\times10^{16}}$ is much higher than that of AlN:$O_{2\times10^{17}}$, which was attributed to the reverse diffusion of implanted ions. In the implantation procedure, vacancy defect was formed, some O^+ions diffused towards the surface of AlN films and then gathered. At the lower implantation doses, less O^+ ions occupied Al vacancies while more O^+ ions occupied Al vacancies at higher doses, leading to the higher vacancy defects at lower implantation doses than higher doses before 60 nm of the film thickness. This anomalous results have also been observed in C^+-implanted AlN films[9]. In the second block of ~350 nm, high S values for AlN:$O_{5\times10^{16}}$ and AlN:$O_{2\times10^{17}}$ are owing to the Al-related vacancies. The third block of ~950 nm depth corresponds to the AlN thickness, the S values tend to be the same due to the annihiltion of vast majority of positrons in the sapphire substrate.

In order to character the change of vacancy type, S–W analysis were performed for all AlN films as shown in Fig. 4. The S–W data for positron energies below 2 keV were subtracted. The fitting curves of the S–W data for the as-grown AlN, AlN:$O_{5\times10^{16}}$, and AlN:$O_{2\times10^{17}}$ are straight lines and approximately overlapped, indicating that these samples contain the same types of defects. Therefore, increasing the

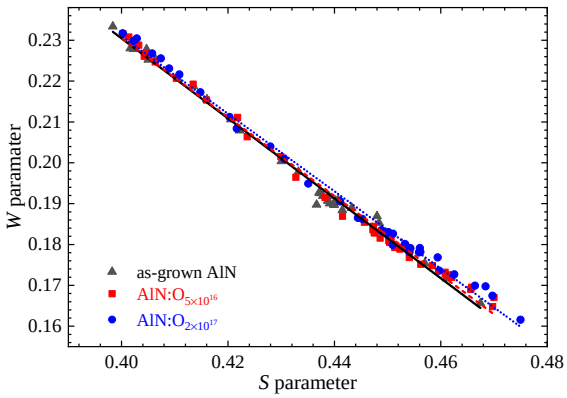

Fig. 4 (Color online) Plots of S vs W for the samples. The black solid, red dashed, and blue dotted lines are fits to the S–W data for the as-grown AlN, AlN:$O_{5\times10^{16}}$, and AlN:$O_{2\times10^{17}}$, respectively.

dose of O^+ ions increases the density of the Al-related vacancies but does not change the defect type.

The variations of magnetization (M) as a function of applied magnetic field (H) for AlN:$O_{5\times10^{16}}$ and AlN:$O_{2\times10^{17}}$ by applying magetic field perpendicular (⊥) to the sample plane are shown in Fig. 5(a). In our previous work, as-grown AlN exhibited an almost zero hysteresis phenomenon and showed diamagnetic character, indicating the absence of magnetic impurities in the as-grown AlN[9]. The ferromagnetic behavior has been observed for AlN:$O_{5\times10^{16}}$ and AlN:$O_{2\times10^{17}}$. The saturation magnetization (M_S) of the AlN:$O_{5\times10^{16}}$ is about 0.68 emu/g, much higher than that of AlN:$O_{2\times10^{17}}$, 0.09 emu/g. This might be due to the excessively high O^+ dose would increase the number of O^+ ions occupying adjacent Al^{3+} positions, resulting in antiferromagnetic coupling[7,23]. This finding is consistent with the DBAR results. The magetic properties of AlN:$O_{5\times10^{16}}$ were measured by applying magnetic field parallel (//) and perpendicular (⊥) to the sample plane, respectively, as shown in Fig. 5(b). Much stronger ferromagnetism of AlN:$O_{5\times10^{16}}$ are observed in the perpendicular diection, 0.68 emu/g than in parallel, 0.29 emu/g. The magnetic anisotropy can be considered as an evidence of intrinsic ferromagnetism in O^+ implanted AlN films[24].

To further investigate origin of the ferromagetism in O^+ implanted AlN films, we calculated their electronic and magnetic properties using the DFT methods[9]. For the supercell containing a single Al vacancy, the total maggetic moment is 3.00 μ_B. Furthermore, the calculated total energy of the spin-polarized state is approximately 556 meV lower than

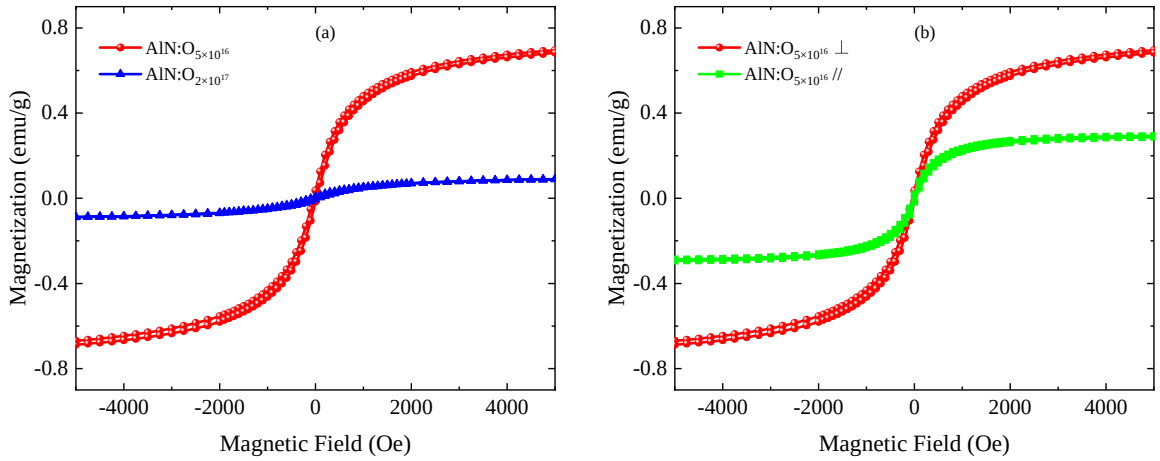

Fig. 5　(Color online) Room-temperature out-of-plane M–H loops for AlN:$O_{5\times10^{16}}$ and AlN:$O_{2\times10^{17}}$. The diamagnetic background signals were subtracted. The magnetization values were normalized by accounting for the masses of the AlN films. (b) Magnetic anisotropy of AlN:$O_{5\times10^{16}}$.

that of the non-spin-polarized state, indicating that single Al vacancy prefers the spin-polarized state. The magnetic coupling of Al divacancies (V_{Al}–V_{Al}) about with different distance are also investigated[25]. The results suggest that the energy difference between antiferromagnetic and ferromagnetic phase rise sharply with distance increasement of two Al vacancies, leading to crucial transformation of V_{Al}–V_{Al} coupling from antiferromagnetism to ferromagnetism. When the V_{Al}–V_{Al} distance is less than 9.96 Å, the magnetic coupling between them is tend to form antiferromagnetic interaction. Thus, for ion-implantation with higher dose, divacancies or vacancy clusters will weaken the ferromagnetism of AlN films, which is consistent with the results of magnetic measurements. According to the above results, it is proposed that the intrinsic ferromagnetism in the O^+ implanted AlN films is related to the Al vacancies. The O^+ ions occupying the adjacent adjacent Al^{3+} positions and Al divacancie or vacancy clusters jointly play an important role in regulating magnetic property in forms of antiferromagnetic alignment.

4　Summary

Room-temperature ferromagnetism was observed in the O^+-implanted AlN films. The saturation magnetization (M_S) was decreased with increasing O^+ dose, due to the excessively high O^+ dose made more O^+ ions occupy adjacent Al^{3+} positions in forms of antiferromagnetic coupling, which was determined by the DBAR experiments. The first-principles calculations and DBAR experiments revealed that the ferromagnetism originates mainly from the Al vacancies.The formation of divacancies or vacancy clusters by high concentrations of Al vacancies will lead to the transformation of V_{Al}–V_{Al} coupling from ferromagnetim to antiferromagnetim, ultimately weakening the ferromagnetism of the sample. This work reveals the roles of cation vacancies and substitute atoms in ferromagnetism within the nonmagnetic element-implanted DMSs. Meanwhile, it demonstrates once more that positron is a very useful probe for nanometer-scaled defects in materials and will be widely used in the research of semiconductors.

5　Acknowledgments

This work was supported by the National Key R&D Program of China (Grant No. 2019YFA0210000), the National Natural Science Foundation of China (Grant No. 12305333), the Fundamental Research Program of Yancheng City (Grant No. YCBK2023061), the State Key Laboratory of Particle Detection and Electronics (Grant No. SKLPDE-KF-202114), the Innovation and Entrepreneurship Doctors of Jiangsu Province (Grant No. JSSCBS20211148), and the Natural Science Foundation of Jiangsu Province (Grant No. BK20220699).

References

[1] ZANG H, SUN X, JIANG K, et al. Advanced Science, 2021, 8(18): 2100100. DOI: 10.1002/advs.202100100.

[2] LIU F, WANG T, GAO X, et al. Science Advances, 2023, 9(31): eadf8484. DOI: 10.1126/sciadv.adf8484.

[3] WOLF S, AWSCHALOM D, BUHRMAN R, et al. Science, 2001, 294(5546): 1488. DOI: 10.1126/science.1065389.
[4] FRAZIER R, STAPLETON J, THALER G, et al. Journal of Applied Physics, 2003, 94(3): 1592. DOI: 10.1063/1.1586987.
[5] KUMAR D, ANTIFAKOS J, BLAMIRE M, et al. Applied physics letters, 2004, 84(24): 5004. DOI: 10.1063/1.1763216.
[6] ZHU Z, OU Z, CHEN Y, et al. Journal of Alloys and Compounds, 2023: 170986. DOI: 10.1016/j.jallcom.2023.170986.
[7] RAN F Y, SUBRAMANIAN M, TANEMURA M, et al. Applied Physics Letters, 2009, 95(11): 112111. DOI: 10.1063/1.3232238.
[8] XU Y, YAO B, LIU D, et al. CrystEngComm, 2013, 15(17): 3271.
[9] YE R, LIU J, ZHANG H, et al. Applied Physics Letters, 2019, 115 (26). DOI: 10.1063/1.5131036.
[10] NATH D, CHAKRAVARTY S, GUPTA M, et al. Journal of Alloys and Compounds, 2023: 171727. DOI: 10.1016/j.jallcom.2023.171727.
[11] TUOMISTO F, MAKKONEN I. Reviews of Modern Physics, 2013, 85(4): 1583. DOI: 10.1103/RevModPhys.85.1583.
[12] AGARWAL S, LIEDKE M, JONES A, et al. Science advances, 2020, 6(31): eaba8437. DOI: 10.1126/sciadv.aba8437.
[13] LIU C, MENSCHING B, VOLZ K, et al. Applied Physics Letters, 1997, 71(16): 2313. DOI: 10.1063/1.120059.
[14] DAVYDOV V Y, KITAEV Y E, GONCHARUK I, et al. Physical Review B, 1998, 58(19): 12899. DOI: 10.1103/PhysRevB.58.12899.
[15] SOARES M, LEITÃO J, DA SILVA M, et al. Optical Materials, 2011, 33(7): 1055. DOI: 10.1016/j.optmat.2010.09.005.
[16] LUGHI V, CLARKE D R. Applied Physics Letters, 2006, 89(24): 241911. DOI: 10.1063/1.2404938.
[17] SHAH A, AHMAD J, AHMAD I, et al. Applied Surface Science, 2014, 317: 262. DOI: 10.1016/j.apsusc.2014.08.112.
[18] ZHANG B, YAO B, LI Y, et al. Applied Physics Letters, 2011, 99 (18): 182503. DOI: 10.1063/1.3657412.
[19] UEDONO A, ITO K, NAKAMORI H, et al. Journal of Applied Physics, 2007, 102(8): 084505. DOI: 10.1063/1.2798586.
[20] LI X, CHEN Z, LIU C, et al. Journal of Applied Physics, 2015, 117 (8): 085706. DOI: 10.1063/1.4913523.
[21] VAN VEEN A, SCHUT H, CLEMENT M, et al. Applied Surface Science, 1995, 85: 216. DOI: 10.1016/0169-4332(94)00334-3.
[22] OKUMURA H, UEDONO A. Japanese Journal of Applied Physics, 2023, 62(2): 020901. DOI: 10.35848/1347-4065/acb898.
[23] XIONG J, GUO P, GUO F, et al. Materials Letters, 2014, 117: 276. DOI: j.matlet.2013.12.018.
[24] VENKATESAN M, FITZGERALD C, LUNNEY J, et al. Phys Rev Lett, 2004, 93(17): 177206. DOI: 10.1103/PhysRevLett.93.177206.
[25] YE R, LIU J, ZHANG H, et al. Room temperature ferromagnetism induced by Al-vacancy in N^+ implanted AlN films[Z].

正电子湮没谱学研究 O 离子注入 AlN 薄膜中缺陷对磁性影响

叶 润[1]，叶邦角[2]

(1. 盐城师范学院物理与电子工程学院, 江苏 盐城 224007；
2. 核探测与核电子学国家重点实验室，中国科学技术大学，安徽 合肥 230026)

摘要：我们在 O 离子注入的 AlN 薄膜 AlN:$O_{5\times10^{16}}$（剂量为 5×10^{16} cm^{-2}）和 AlN:$O_{2\times10^{17}}$（剂量为 2×10^{17} cm^{-2}）中观察到了室温铁磁性。所观察到的磁各向异性表明，O 离子注入的 AlN 薄膜中铁磁性是本征特性。在垂直于样品平面的外加磁场下，AlN:$O_{5\times10^{16}}$ 中的饱和磁化强度约为 0.68 emu/g，高于 AlN:$O_{2\times10^{17}}$ 中的饱和磁化强度 0.09 emu/g。这是由于过高的 O 离子剂量使得更多的 O 离子占据相邻的 Al 离子位置，导致了反铁磁耦合的出现。正电子湮没多普勒展宽谱表明在 O 离子注入的 AlN 薄膜中存在大量的 Al 空位。第一性原理计算表明 O 离子注入的 AlN 薄膜中的铁磁性主要来源于 Al 空位，而高浓度的 Al 空位形成双空位或空位团将会使得 AlN 样品从铁磁性到反铁磁性转变，最终使样品的铁磁性减弱。

关键词：正电子湮没谱学；离子注入；半导体；铁磁性

收稿日期：2024-04-01；　**修改日期：**2024-04-01

基金项目：国家重点研发计划“纳米科技”重点专项资助 (2019YFA0210000)；国家自然科学基金资助 (12305333)；核探测与核电子学国家重点实验室开放课题资助 (SKLPDE-KF-202114)；盐城市基础研究计划资助 (YCBK2023061)；江苏省“双创博士”计划资助 (JSSCBS20211148)；江苏省自然科学基金资助 (BK20220699)

通信作者：叶润，E-mail: yer@yctu.edu.cn

通信作者：叶邦角，E-mail: bjye@ustc.edu.cn